AGU PUBLICATIONS

JGR

Journal of Geophysical Research: Space Physics

RESEARCH ARTICLE
10.1002/2015JA021669

Key Points:
- Parallel-dominant and perpendicular-dominant components of the fast bulk flows
- Ion distribution of the fast bulk flow near the current sheet
- Relationship between the fast bulk flow and the PSBL beams

Correspondence to:
L. Q. Zhang,
lqzhang@nssc.ac.cn

Citation:
Zhang, L. Q., L. Dai, W. Baumjohann, H. Rème, M. W. Dunlop, and X. H. Wei (2015), Parallel-dominant and perpendicular-dominant components of the fast bulk flow: Comparing with the PSBL beams, *J. Geophys. Res. Space Physics*, *120*, 9500–9512, doi:10.1002/2015JA021669.

Received 11 JUL 2015
Accepted 22 OCT 2015
Accepted article online 26 OCT 2015
Published online 18 NOV 2015

Parallel-dominant and perpendicular-dominant components of the fast bulk flow: Comparing with the PSBL beams

L. Q. Zhang[1], L. Dai[1], W. Baumjohann[2], H. Rème[3,4], M. W. Dunlop[5,6], and X. H. Wei[1]

[1]State Key Laboratory of Space Weather, National Space Science Center, Chinese Academy of Sciences, Beijing, China, [2]Space Research Institute, Austrian Academy of Sciences, Graz, Austria, [3]UPS-OMP, IRAP, University of Toulouse, Toulouse, France, [4]CNRS, IRAP, Toulouse cedex 4, France, [5]Space Research Institute, School of Astronautics, Beihang University, Beijing, China, [6]Space Sciences Division, Rutherford Appleton Laboratory, Chilton, UK

Abstract Utilizing multipoint observations by the Cluster satellites, we investigated the ion distributions of the fast bulk flows (FBFs) in the plasma sheet. Simultaneous observation by C1 and C3 revealed that parallel-dominant and perpendicular-dominant components of the flows coexist and correspond to B_x-dominant and B_z-dominant magnetic field regions within the FBFs, respectively. In both cases, the ions distributions are characterized by a single-beam/crescent shape. In particular, no reflected ions are found within the FBFs. Statistical analysis showed that within the FBFs, the strength of the B_x component is typically less than 5 nT for B_z-dominant regions and above 10 nT for B_x-dominant regions. To distinguish between the parallel-dominant component of the FBFs and the field-aligned beams in the plasma sheet boundary layer (PSBL), we further statistically analyzed the tailward parallel flows (TPF) with positive B_z in the plasma sheet. The results indicated that the FBFs tend to have higher velocity, weaker B, and higher magnetic tilt angle (θ_{MTA}) than the TPFs/PSBL beams. Statistically, in the region of $B > 30$ nT ($\theta_{MTA} > 10°$), only PSBL beams can be observed, while in the region of $B < 10$ nT ($\theta_{MTA} > 30°$), the FBFs are dominant. In the intermediate region ($10° < \theta_{MTA} < 30°$) of the plasma sheet, the FBFs and the PSBL beams cooccur. These Cluster observations suggest that the X line can produce both perpendicular flow in central plasma sheet and parallel flow in the PSBL. In addition, the parallel-dominant component of the FBFs could be an important origin for the PSBL beams.

1. Introduction

Fast flows in the plasma sheet play a dominant role in mass and energy transport in the magnetotail [*Angelopoulos et al*., 1994; *Schödel et al*., 2001; *Baumjohann*, 2002; *Zhang et al*., 2009]. They often occur during substorms [*Akasofu*, *et al*., 1981; *Hones*, 1973; *Lui et al*., 1977a, 1977b; *Lui et al*., 1983] and may result from current disruption in the near-Earth region, as outflows from near-Earth reconnection, or from the distant tail neutral line [*Lui*, 1991; *Baker et al*., 1996; *Lui*, 1996; *Shiokawa et al*., 1998; *Nakamura et al*., 2001a, 2001b; *Angelopoulos et al*., 2008; *Nishimura et al*., 2011; *Lyons et al*., 2012; *Angelopoulos et al*., 2013; *Zhang et al*., 2015a].

According to *Baumjohann et al*. [1990], the fast observed flows exceeded 400 km/s for less than 10 s. Such short life-time fast flows are also called bursty flows. The bursty fast flows are typically convective in the central plasma sheet (CPS) and parallel in the plasma sheet boundary layer (PSBL). *Angelopoulos et al*. [1992] found that the convective bursty flows in the inner CPS are usually groups which had durations of up to 10 min. These grouped bursty flows are also named as bursty bulk flows (BBFs). BBFs are mainly considered as signatures of instantaneous, localized magnetic reconnection in the near-Earth magnetotail [e.g., *Nagai et al*., 1998; *Zhang et al*., 2010].

Fast flows in the CPS and the PSBL can be easily distinguished from each other according to the angles between the velocity of the ions and the magnetic field (θ_{VB}) [*Paterson et al*., 1998; *Petrukovich et al*., 2001]. However, their relationship is still under debate [*Birn et al*., 1986; *Schindler and Birn*, 1987; *Angelopoulos et al*., 1993; *Raj et al*., 2002; *Birn et al*., 2004; *Lennartsson et al*., 2009]. On one hand, they do exhibit several common properties, including: similar proton flux, energy, hot ion density, time scale, and occurrence [*Baumjohann et al*., 1990; *Lennartsson et al*., 2001, 2009]. On the other hand, the FBF and the PSBL beams have

different field strengths, magnetic tilt angle, and ion distributions [*Baumjohann et al*., 1988, 1989; *Nakamura et al*., 1991, 1992]. Utilizing Wind observations, *Raj et al*. [2002] statistically analyzed the ion distributions of all the fast flows in the plasma sheet. They found that fast flows in the plasma sheet can be divided into two categories: the bulk flow and field-aligned beams. The bulk flow can be observed in both the CPS and the PSBL. The bulk flow is perpendicular to the magnetic field in the CPS but has a large field-aligned component in the PSBL. The bulk flows in the CPS and the PSBL have the same isotropic ion distribution, while the field-aligned flows in the PSBL have the beam-like ion distribution with a low-energy cutoff.

Ion velocity distributions contain important information to help understanding the origins of the fast flows in the plasma sheet. Typically, the convective fast flows in the CPS have "kidney bean" or isotropic shape ion distributions, while the parallel fast flows in the PSBL are characteristic of single-beam or double-beam ion distributions [*Sarris et al*., 1978; *Takahashi and Hones*, 1988; *Williams*, 1981]. Traditionally, the PSBL beams are thought to be produced by the far-tail X lines [e.g., *Ashour-Abdalla et al*., 1991; *Nakamura et al*., 1992; *Onsager et al*., 1991; *Grigorenko et al*., 2007, 2009], while the isotropic shape ion distributions associated with the convective fast flows in the CPS are generated by the near-Earth X lines [*Angelopoulos et al*., 1989; *Nakamura et al*., 1991; *Raj et al*., 2002].

The PSBL is an important dynamic region where the magnetic field lines are directly connected to the auroral region [*DeCoster and Frank*, 1979; *Lyons et al*., 2010]. *Lui et al*. [1977a, 1977b] first found that a large number of fast flows in the PSBL exist. These fast flows move mainly along the magnetic field lines in both earthward and tailward directions [*Williams*, 1981; *Green and Horwitz*, 1986; *Angelopoulos et al*., 1989]. Reflected beams at the magnetic mirror point can account for tailward parallel flows (TPFs) in the PSBL [*Andrew et al*., 1981; *Eastman et al*., 1984, 1985; *Zhang et al*., 2015b].

The organization of this paper is as follows. In section 2, we show three typical ceases. Case 1 shows the simultaneous observation of the parallel-dominant and perpendicular-dominant components in the same FBF by C1 and C3. Case 2 shows the spatial evolution of the ion distribution from parallel-dominant to perpendicular dominant within the FBF observed by C3. Case 3 shows the transition of the ion distributions of the PSBL beam from earthward to tailward. In section 3, we present the data used in this study and the selection criterion of the FBFs and the TPFs as well. Section 4 shows the statistical analysis of the internal structure of the ions and the magnetic field in south-north direction within the FBF. In section 5, we statistically analyze and compare the properties of the FBFs with the TPFs. In section 6, we discuss the possible formation mechanism for the coexistence of parallel-dominant and perpendicular-dominant components within the FBFs. In addition, the explanation of the scarcity of the reflected ions inside the FBF is given. Conclusions are provided in section 6.

2. Case Studies

2.1. Simultaneous Observations by C1 and C3

A strong FBF appeared at 23:43 UT on 07 August 2001. The corresponding temporal evolution of the magnetic field and ions are shown in Figure 1. The two flows observed by C1 and C3 have similar velocity, and high ion temperature (~40 MK), and low ion density (~0.1 cm^{-3}). Before and after the flow, C1 and C3 are both located in the outer plasma sheet (OPS) where B_x component is about 20 nT. In the following period the flow, strong magnetic field fluctuations are present at both C1 and C3 locations. The B_x component at the C1 location remains positive and is mainly above 10 nT, while the B_x component at the C3 location becomes negative and the absolute value is mainly less than 10 nT.

At 23:45:45 (marked by the dashed line), C1 is located at ($-17.1\ R_E$, $-8.4\ R_E$, $2.2\ R_E$) and C3 is located at ($-17.3\ R_E$, $-8.3\ R_E$, $2.0\ R_E$). The B_x component is almost zero for C3, and 12 nT for C1. The B_z component is almost zero for C3, and 5 nT for C1. Clearly, C1 is located in the CPS, while C3 is located in the OPS. The magnetic field is B_z-dominant for C3 and B_x-dominant for C1. The angle θ_{VB} is nearly 90° at C3, and about 140° at C1. Thus, the FBF is perpendicular-dominant at C3, and parallel-dominant at C1.

The simultaneous ion distributions observed by C1 and C3 at 23:45:45 are shown in Figure 2. The ion distributions in both the V_{xy} and V_{xz} planes at C1 and C3 are almost the same. Both are beam-like with a low-energy cutoff (lack of ions in the low-velocity regime in the V_{xy} and V_{xz} planes). Both are single-beam/crescent shape. Moreover, both positions of the peak ion density (PID) are located at V_x axis. The similarity in the ion distributions implies that the ion motion remains consistent at C1 and C3. Ion motions at C1 and C3 are both directed mainly toward the Earth.

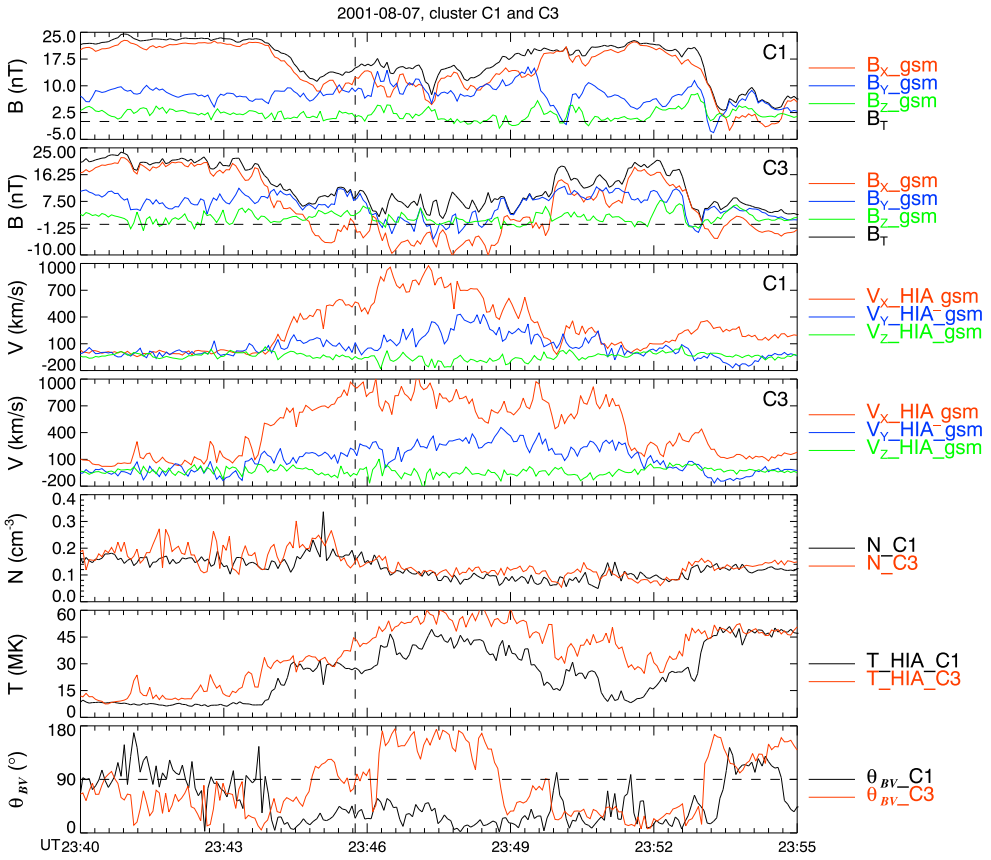

Figure 1. The fast flows simultaneously observed by C1 and C3 on 07 August 2001. First and second panels show the magnetic field observed by C1 and C3. Third and fourth panels show the plasma velocities observed at C1 and C3. Fifth to seventh panels are the ion density, ion temperature, and the angle between the flow velocity *V* and the magnetic field *B*, respectively. Corresponding to the dashed line, B_x remains large at C1 but switches sign at C3, demonstrating C3 crossing the CPS. Positive V_x (red) indicate fast earthward flow simultaneously observed by C1 and C3.

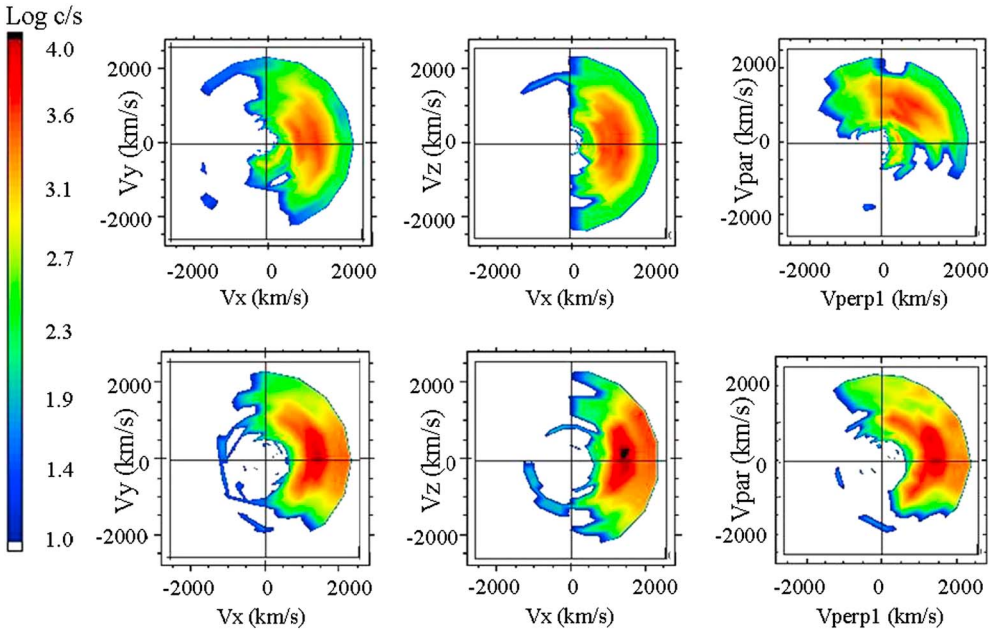

Figure 2. The ion distributions at 23:45:45 by C1 (upper) and C3 (bottom).

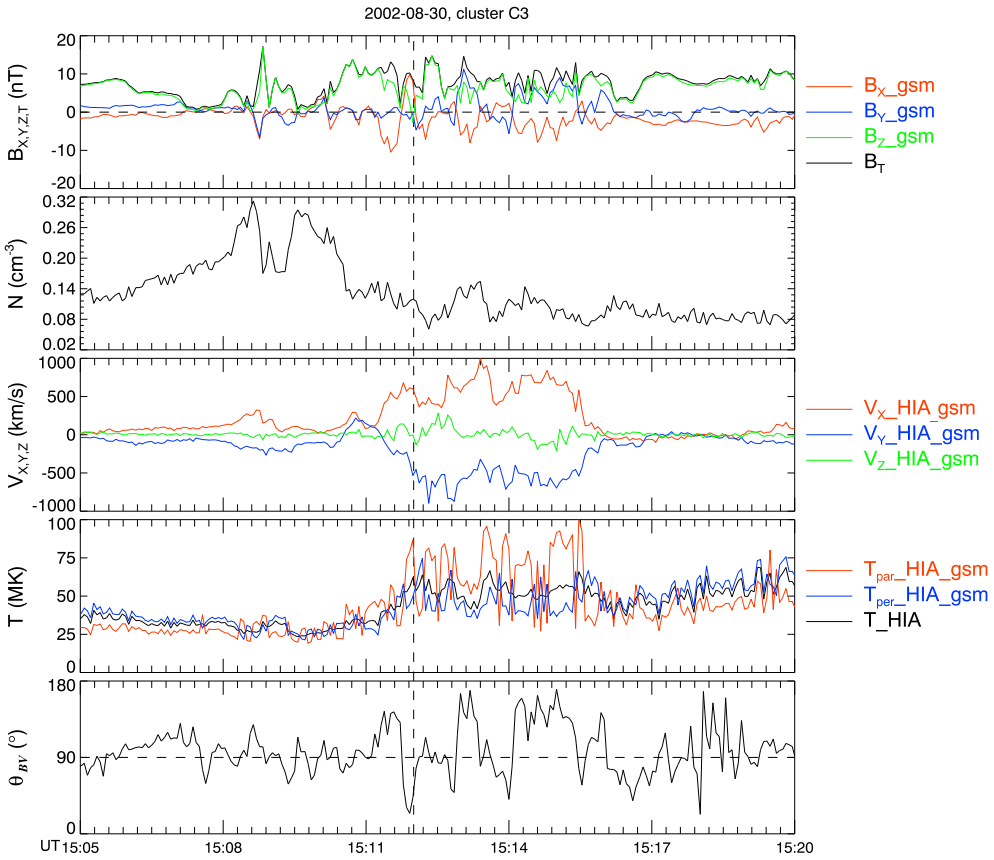

Figure 3. The fast flow near the current sheet on 30 Aug, 2002 observed by C3 From top to bottom, the panels are respectively magnetic data (B_x, B_y, B_z, and total B), ion density, the three components of the velocity, temperature, and the angle between the flow and the magnetic field. The dashed line indicates the time when C3 is crossing the current sheet.

In the $V_{\parallel}$-$V_{\perp 1}$ plane, the ion distributions at C1 and C3 are also quite similar. Both are crescent shape. However, the positions of the PID are distinctly different. The position of the PID is located close to the $V_{\parallel}$ axis at the C1 location and to the $V_{\perp}$ axis at the C3 location. This is consistent with the observed parallel-dominant and perpendicular-dominant components at C1 and C3, respectively.

Combined ion distributions in Figure 2 indicate that the difference of the θ_{VB} between C1 and C3 is due to the variation of the direction of the magnetic field B. According to Figure 1, the magnetic field is B_x-dominant and the direction of the magnetic field is Sun-Earth directed at C1. Meanwhile, the magnetic field is B_z-dominant, and the direction of the magnetic field is mainly in the south-north direction at C3. As a consequence, the earthward-moving FBF is perpendicular-dominant at C3, and parallel-dominant at C1.

It is worth noting that a double-layer structure exists in the ion distribution in Figures 2. Such multiple-layer structure can occasionally be seen in the FBF near the current sheet. Each layer is beam shaped. We checked the associated-energy distribution of the different ion species. It seems that the number of other ion species is too low to affect the ion distribution. In addition, the multiple-layer structure always shows a single peak, but with a very broad energy range of the ions from several hundred eV to above several tens of keV (not shown here). It appears that the count rate of the ions in certain energy range may be lower than that in the others, which then causes the double- or multiple-layer structure in the ion distributions.

2.2. FBF Near the Current Sheet

Typically, the B_z-dominant magnetic field appears in and/or near the current sheet. To understand the spatial evolutions of the ions and the magnetic filed inside the FBF in the north-south direction, we further analyzed the ion distributions of the FBFs near the current sheet.

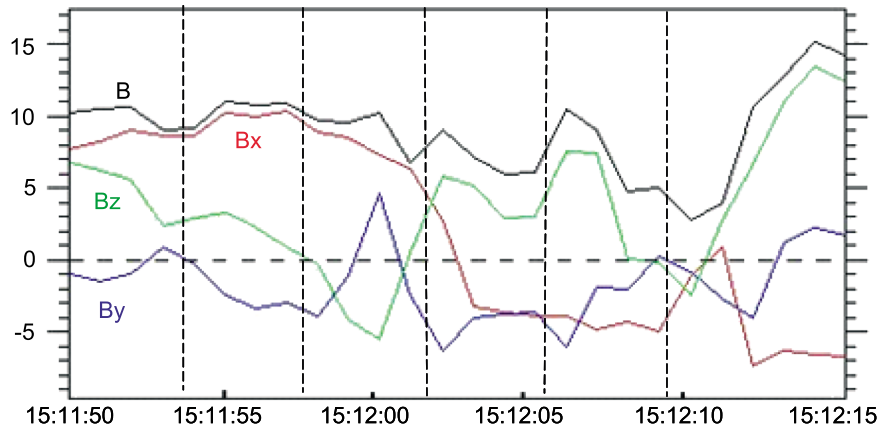

(a). The temporal evolutions of the magnetic field from 1s-resolution FGM data

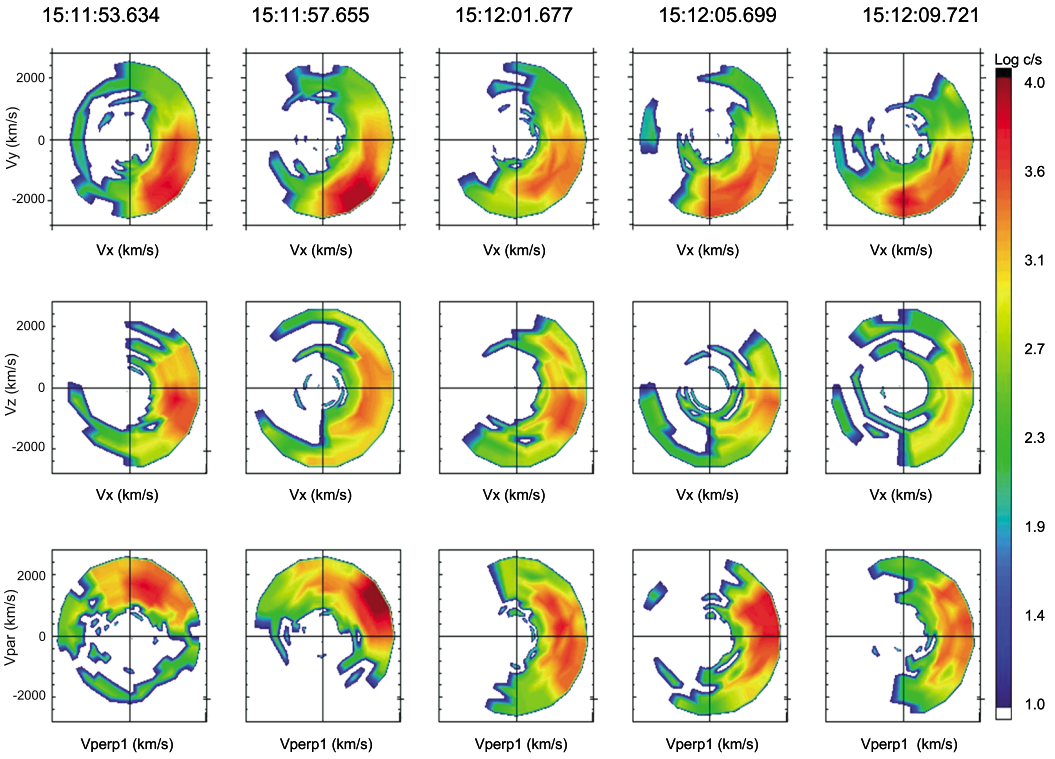

(b). Ion distributions (taken at times denoted by the dashed lines in Figure 4(a))

Figure 4. (a) The temporal evolutions of the magnetic field from 1 s resolution FGM data. (b) Ion distributions (taken at times denoted by the dashed lines in Figure 4a).

A strong FBF near the current sheet event was observed by C3/Cluster on 30 August 2002. The temporal evolution of the magnetic field and ions in the FBF (in GSM coordinates) is shown in Figure 3. The FBF continues from 15:07 UT to 15:16 UT. In this interval, C3 was located near midnight at X ~ −18.6 R_E. The magnitude of the total B associated with the fast flow is weak and mostly less than 10 nT. The B_x component experienced several reversals which indicate that C3 crossed the current sheet several times. The maximum velocity of the flow exceeded 1000 km/s. The dominant ion component associated with the flow has a low density less than 0.1 cm^{-3} and a high temperature about 40 keV. The angle between the flow velocity and the magnetic field (θ_{VB}) strongly fluctuated between 40° and 160°. As a whole, the FBF has a significant parallel component.

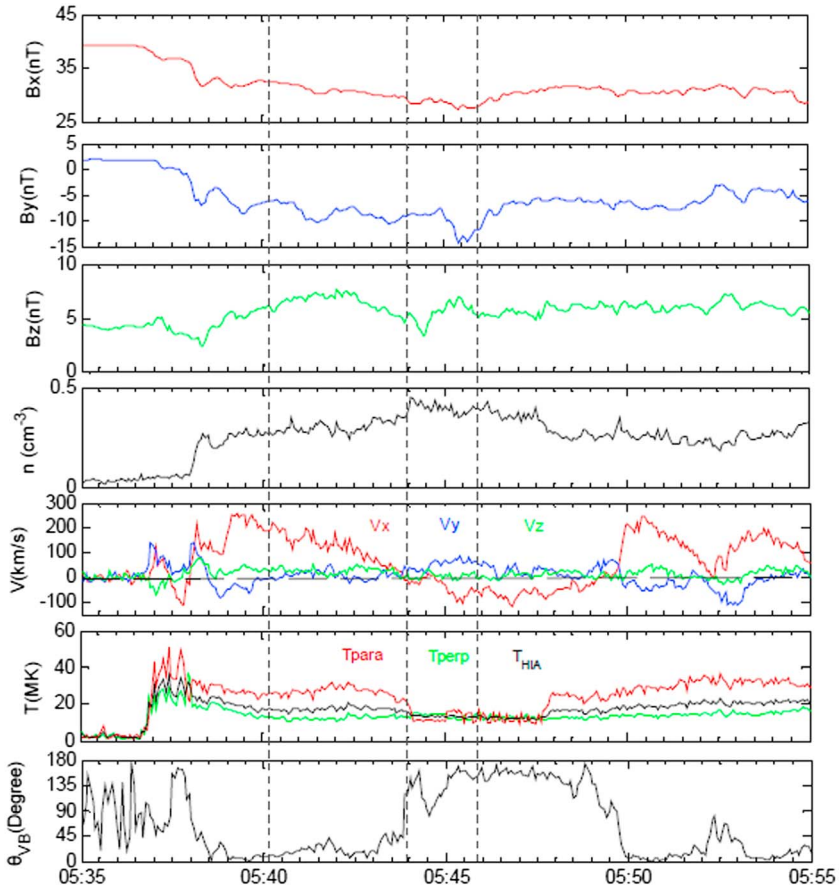

Figure 5. The bidirection beams in the PSBL on 18 August 2006. The dashed lines corresponds to the earthward, absence, and tailward beams, respectively.

Around 15:12 (denoted by the dashed line), the B_x component at C3 is almost zero. C3 crosses the current sheet from the north hemisphere to the south hemisphere. We choose this crossing to do the analysis.

The 1 s resolution FluxGate Magnetometer (FGM) data in the period from 1511:50 UT to 1512:15 UT (corresponding to the dashed line in Figure 3) is shown in Figure 4a. In this interval, the B_y and B_z components strongly fluctuate, which is consistent with an Alfvén wave, and/or the turbulent magnetic field near the reconnection site [*Nakamura et al*., 2006; *Dai et al*., 2011]. The B_x component gradually changed from 10 nT to −5 nT. The B_z components mainly change around zero with an absolute values less than 5 nT. The direction of the magnetic field gradually changed from B_x-dominant to B_z-dominant. In particular, B_x was almost zero around 1512:01 UT as C3 crosses the current sheet.

The corresponding 4 s resolution ion distribution from 15:11:54 UT to 15:12:19 UT is shown in Figure 4b. The ion distribution is characterized by a single component beam-like shape with low-energy cutoff in the V_x-V_y and V_x-V_z planes (GSM coordinates). The crescent-shape of the ion distribution remains almost unchanged in this interval. The position of the peak ion density is located close to the positive V_x axis, which is consistent with earthward moving thermal ions. Similarly, the ion distributions in the $V_{\parallel}$-$V_{\perp 1}$ plane are also beam-like with a low-energy cutoff. However, the position of the peak ion density continuously moves from $V_{\parallel}$ axis to $V_{\perp 1}$ axis. Correspondingly, the flow gradually changes from being parallel-dominant to being perpendicular-dominant.

Combined magnetic field and ion distributions in Figure 4 clearly showed that within the FBF, the magnetic field has gradually changed from B_z-dominant (south-north direction) to B_x-dominant (Sun-Earth direction) while away from the neutral sheet. Along with the evolution of the magnetic field, the FBF gradually changes from perpendicular-dominant to parallel-dominant. As a whole, θ_{VB} depends

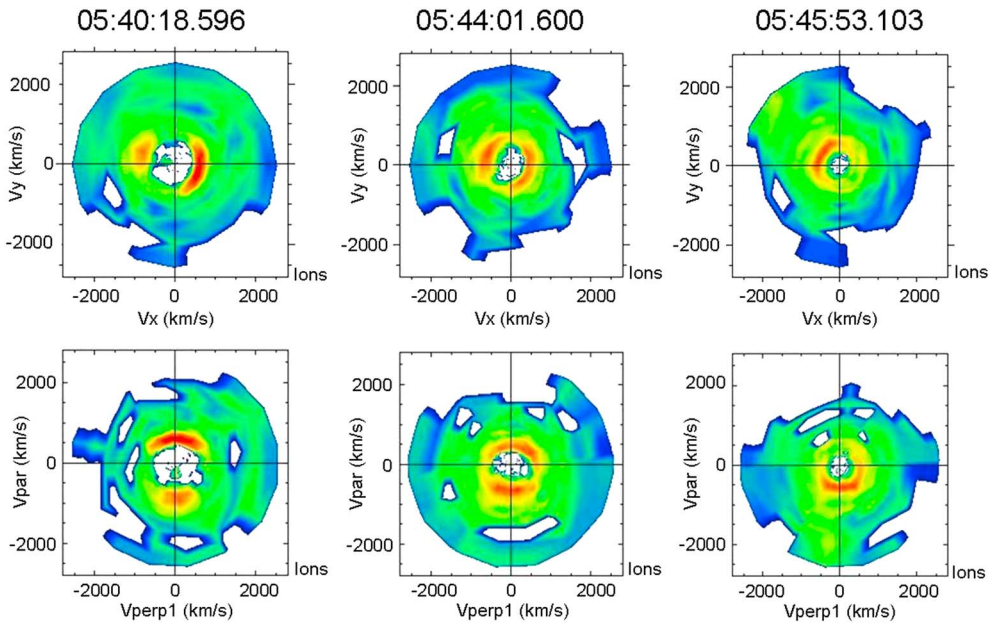

Figure 6. Ion distributions corresponds to the different states of the beams denoted by the three dashed lines in Figure 5, respectively.

on the direction of the magnetic field, which is predominantly determined by the magnitude of the B_x component.

2.3. Bidirection Beams in the PSBL

A typical bidirection beam event in the PSBL on 18 August 2006 was recorded by C3. Corresponding temporal evolutions of the magnetic field and the hot ions from 05:35 UT to 05:55 UT are shown in Figure 5. The magnitude of B_x component is about 30 nT. This indicates that C3 is located in the PSBL. The fast earthward flow begins at 05:36. The velocity of the flow reaches the peak (~250 km/s) at 05:39. The velocity is almost zero at 05:44. Afterward, a tailward fast flow is observed.

The ion distributions related to the beam are shown in the Figure 6. The three ion distributions correspond to the earthward fast flow, the zero-velocity interval, and the tailward fast flow, respectively. All the three ion distributions are characterized by the double-beam shape with low energy cutoff. At 05:40:19 UT, the ion density of the beam is much stronger in the positive $V_{\|}$ axis than in the negative $V_{\|}$ axis. The flow moves earthward. At 05:44:02 UT, the ion densities of the two beams are almost equal. The resulting velocity moment is almost zero. At 05:45:53 UT, the flow moves tailward. The density is higher in the negative $V_{\|}$ direction because more ions are flowing tailward than earthward.

3. Flow Selections

The 4 s resolution data of the magnetometer FGM [*Balogh et al.*, 2001] and the plasma analyzer HIA data [*Rème et al.*, 2001] on C3 were collected from 2001 to 2006. The selection region is chosen to be inside a box of $-19\ R_E < X < -10\ R_E$, $-10\ R_E < Y < 10\ R_E$ and $-6\ R_E < Z < 6\ R_E$ (in the GSM coordinates).

The selection criterion of a FBF event is that: the duration time of $V_x > 200$ km/s exceeds 20 s and $B_z > 0$ and $45° < \theta_{VB} < 135°$. There are in total 424 FBF events selected.

To ensure that the selected parallel fast flows are PSBL beams, we use tailward parallel flows (TPF) in this study. The selection criterion of the TPF is adopted as that: the duration time of $V_x < -200$ km/s exceeds 20s and $B_z > 0$ and $\theta_{VB} < 45°$ or $> 135°$. From 2001 to 2006, there are 167 TPF events selected in total. To verify if the selected TPFs are PSBL beams, we checked the ion distributions of all 167 TPFs events. The ion distributions of all TPFs events are characteristic of the double beams. Clearly, the selected TPFs are the PSBL beams.

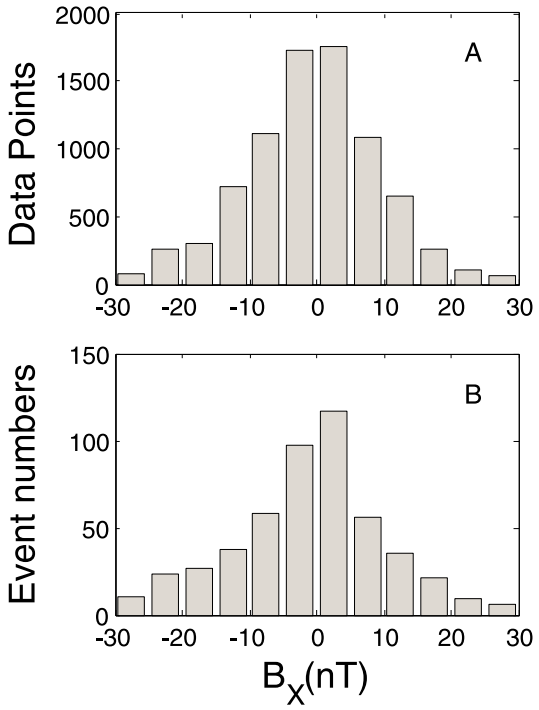

Figure 7. (a) Data points versus B_x. (b) Events number versus B_x. Totally, 8275 points of 4 s resolution effective data points are collected from all FBF events. Then, all the data points are arranged into small bins with a step of 5 nT.

4. Internal Structure of the FBF

4.1. B_x Within the FBF

The 4 s resolution data points of the ions and the magnetic field of all FBF events in the period of $V_x > 200$ km/s are collected. There are in total 8275 data points. Each data point within the FBF is arranged into small bins with a step of 5 nT.

The distribution of the data point number with B_x is shown in Figure 7a. The data points have a wide distribution from −30 nT to 30 nT. The distribution of the data points is quite symmetric. This suggests that the structure of the FBF is symmetric on the two sides of the current sheet. Most of the data points are located in the weak magnetic region of B_x less than 15 nT.

The distribution of the event number with B_x is shown in Figure 7b. The magnitude of $|Bx|$ within the FBF has a wide distribution from 0 to 25 nT. In addition, the occurrence peaks in the neutral sheet where $|Bx|$ is less than 5 nT. The occurrence decreases sharply with B_x increasing. This is related to the crossing-orbit of C3 within the FBF shown in Figure 7a.

4.2. θ_{VB} versus B_x

The distribution of the angle between the bulk velocity and the magnetic field (θ_{VB}) with B_x for each data point is shown in Figure 8. The variations of θ_{VB} with B_x in the northern hemisphere and southern hemisphere have similar tendency. The magnetic field within the FBF can be divided into three different regions depending on the variation of the θ_{VB}:

1. The B_z-dominant region: corresponding to the regime of $|B_x| < 5$ nT. In this region, the magnetic field is mainly in the north-south direction. The averaged θ_{VB} sharply decreases with B_x increasing from 90° to 60° in the northern hemisphere and increases with B_x decreasing from 90° to 120° in the southern hemisphere. The perpendicular component is dominant.

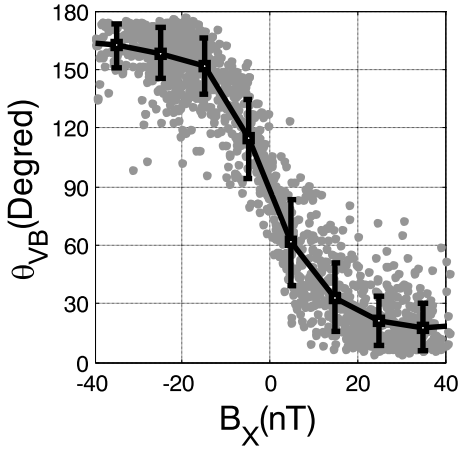

Figure 8. θ_{VB} versus B_x.

2. The B_x-dominant region: corresponding to the regime of $|Bx| > 10$ nT. In this region, the magnetic field is mainly in the Sun-Earth direction. The averaged θ_{VB} tends to slowly increase with the absolute value of B_x increasing. As $|Bx|$ increases from 10 nT to 40 nT, the average value of the θ_{VB} varies from about 50° to 20° in the northern hemisphere, and from 130° to 160° in the southern hemisphere. The parallel component is dominant.
3. The intermediate region: corresponding to the residual regime of 5 nT $< |B_x| < 10$ nT. In this region, the magnetic field varies from B_z -dominant to B_x-dominant, and the FBF is gradually translated from perpendicular-dominant to parallel-dominant. The θ_{VB} rapidly decrease/increase with B_x increasing in the northern/southern hemisphere.

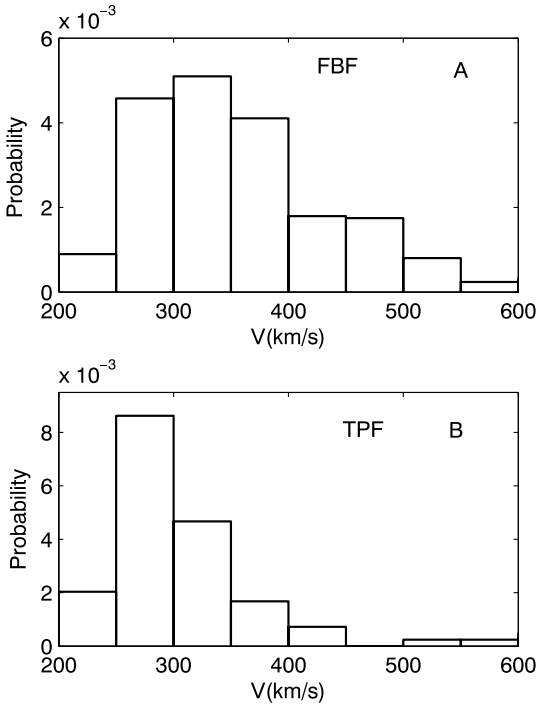

Figure 9. Probabilities of velocity.

5. Comparing FBF With TPF

The 4 s resolution data points are collected for each FBF/TPF over its duration. The flow velocity and other physical parameters in each FBF/TPF event are defined as average values over the event duration.

5.1. Velocity

The probability of the bulk velocity (V) of the FBF is shown in Figure 9a. The value of the velocity has a wide range from 250 km/s to 500 km/s. The most probable TPF velocity observed is about 300 km/s.

The probability of the bulk velocity, V, of the TPF is shown in Figure 9b. The probability of the TPF peaks around 300 km/s. Above 250 km/s, the probability of the TPF decreases rapidly with V increasing. The TPF seldom have higher velocity above 450 km/s. Comparing with Figure 9a, the FBF clearly tend to have a higher velocity than the TPF.

5.2. Magnetic Field

The probability of the magnetic field (B) values of the FBF is shown in Figure 10a. The occurrence is distributed dominantly between 5 nT and 25 nT with peaks around 10 nT. Seldom FBF occur for B above 25 nT. This is basically consistent with the previous results [e.g., *Baumjohann et al.*, 1990].

The probability of B values of the TPF is shown in Figure 10b. The occurrence is distributed dominantly between 10 nT and 35 nT with the peak around 25 nT. A certain number of TPF events have stronger B than 40 nT. Comparing with Figure 10a, the TPF is dominant flow in the region of B above 20 nT and the FBF is dominant in the region of B below 20 nT.

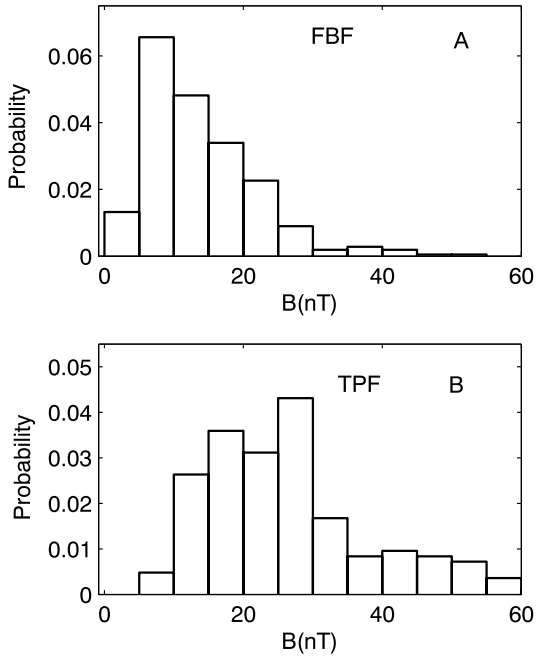

Figure 10. Probabilities of B.

5.3. θ_{MTA}

The magnetic tilt angle (θ_{MTA}) is calculated as $\arctan\left(B_z/\sqrt{\left(B_x^2+B_y^2\right)}\right)$. The probability of θ_{MTA} values of the FBF is shown in Figure 11a. The θ_{MTA} has a wide distribution from 0° to 90°. Most of the FBFs occur between 5° and 35°. Below 35°, the occurrence of the FBF has no clear change. Above 35°, the occurrence of the FBF has a sudden decrease.

The probability of θ_{MTA} values of the TPF is shown in Figure 11b. The θ_{MTA} predominantly varies between 0° and 30°. The TPF seldom occur for θ_{MTA} above 30°. The occurrence of the TPF rapidly decreases with the θ_{MTA} increasing. Comparing with Figure 8a, in the region of $\theta_{MTA} < 30°$, both TPF and FBF occur. However, in the region of $\theta_{MTA} > 30°$, only FBF can be observed.

From analysis above, the FBF tend to have a higher velocity, weaker B and higher θ_{MTA} than

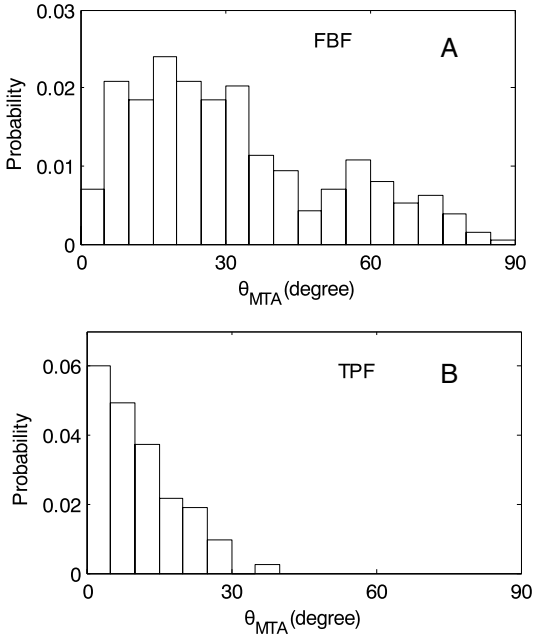

Figure 11. Probabilities of $\theta_{(MTA)}$.

the TPFs/PSBL beams. In the region of $B > 30$ nT and/or $\theta_{MTA} < 10°$, only PSBL beams can be observed. While in the region of $B < 10$ nT and/or $\theta_{MTA} > 30°$, the FBF is dominant. In the intermediate region (10 nT $< B <$ 30 nT), the FBF and the PSBL beams coexist.

6. Discussion and Conclusions

Most FBFs include perpendicular and parallel components. Previous studies showed that the FBFs in the CPS are typically perpendicular-dominant, and their parallel components are quite small [*Baumjohann et al*., 1989, 1990; *Petrukovich et al*., 2001]. In this study, we have shown that C1 observe a clear perpendicular-dominant component and C3 observed a clear parallel-dominant component within the same FBF. The perpendicular-dominant and parallel-dominant components are located in the weak- B_x and strong-B_x magnetic field regions, respectively. This has never been reported before as far as we know. It suggests the X line (at least at times) produces perpendicular flow in the CPS and parallel flow in the PSBL.

A second interesting result of this paper concerns the beam-like or crescent shape of the ion distribution of the FBF. Traditionally, such a shape of the ion distribution was thought to occur only in the PSBL [*Nakamura et al*., 1992, *Raj et al*., 2002]. The perpendicular-dominant component within the FBF was especially found to have such beam-like ion distributions near the CPS. Our result suggests that near-Earth magnetic reconnection could produce the crescent shape of the ion distribution in both the CPS and the OPS/PSBL (a somewhat related study [Hietala et al., accepted], which just appeared online, independently came to a similar conclusion).

The simultaneous observations of the PSBL beams and the bursty flows near the current sheet have been reported by *Zhou et al*. [2012]. However, in their study (Figure 2 in *Zhou et al*. [2012]), the ion distribution has two different components. One is isotropic and the other is beam-like which correspond to the bursty flow and PSBL beam, respectively. The ion energy of the beam is distinctly higher than the isotropic component, and the bursty flow and the beam have different origins. Hence, the simultaneous beam in *Zhou et al*. [2012] is not the parallel component within the FBF as presented here, but instead the PSBL beam.

Simultaneous observations by C1 and C3 reveal that the B_x-dominant and B_z-dominant magnetic field regions can coexist in the same flux tube. This implies that the FBF should have larger thickness than the thin current sheet in the outflow region. The thin current sheet is usually formed during the late growth and expansion phase of a substorm in the near-Earth region with a thickness from 500 km to 1 R_E [*Petrukovich et al*., 2007; *Nakamura et al*., 2008]. Furthermore, the scale of the current sheet near the magnetic reconnection region could be less than 1000 km, which is on the same order of ion inertial length or ion gyroradius [*Runov et al*., 2003; *Nakamura et al*., 2002, 2006; *Dai et al*., 2015]. Our results show that the fast flow in the outflow region could be wider than the current sheet thickness, occupying the B_x-dominant and B_z-dominant magnetic field regions at the same time.

Based on multipoint analysis, *Nakamura et al*. [2004] found that the width of the BBF is 1.5–2 R_E in the north-south direction. Probably, the FBF could intrude into the PSBL, and the parallel component could be an important genesis of the beams in the PSBL. In addition, the braking of the convective flows in the near-Earth region could also turn the FBF into the PSBL beams. Here we suggest that the parallel component of the FBF could be an important origin of the PSBL beams.

From the case analysis, we noticed that the parallel component within the FBF is characteristic of a single-beam structure, while the PSBL beams are typically double-beams structures. To answer the question whether the parallel component within the FBF could also be reflected back, we manually checked the ion distributions of all 424 FBF events case by case. No double-beam ion distribution was found. In other words, no reflected ions can be seen inside the FBF.

Usually, beam ions moving along the magnetic field lines would be lost to the ionosphere/atmosphere due to the precipitation [*Ashour-Abdalla et al*., 1992]. However, the precipitation of the ions can not explain the scarcity of the reflected ions within the FBF. Our explanation is that nonreflected ion within the FBF is related with the bulk motion of the FBF. All ions within the FBF, including the parallel-dominant and perpendicular-dominant ion components, move together in the same velocity toward the Earth. This can be clearly seen from the ion distribution of the FBF. The perpendicular-dominant component would stop/brake in the near Earth region (between 13 and15 R_E) [*Shiokawa et al*., 1997]. Afterward, the FBF could be possibly turned into PSBL beam in the deceleration/braking region because the parallel-dominant component was not affected by the braking. Thus, the reflected ions of the parallel component could not be directly observed inside the FBF before the braking.

In conclusion, we found cases in which both the perpendicular-dominant and parallel-dominant components of the flow, corresponding to the B_z-dominant and B_x-dominant magnetic field, respectively, coexist inside the FBF. Statistical analysis showed that the strength of the B_x component within the FBF is typically less than 5 nT for B_z-dominant region and above 10 nT for B_x-dominant region. Further analysis showed that the FBF tends to have higher velocity, weaker B and higher θ_{MTA} than the PSBL beam. Typically, in the region of $B > 30$ nT and/or $\theta_{\mathrm{MTA}} < 10°$, only PSBL beams can be observed. While in the region of $B < 10$ nT and/or, $\theta_{\mathrm{MTA}} > 30°$, the FBF is dominant. In the intermediate region ($10° < \theta_{\mathrm{MTA}} < 30°$), the FBF and the PSBL beams coexist.

Acknowledgments

We thank the Toulouse CIS/Cluster team for supplying the Cluster data used in this paper. The data of Cluster used in this paper are available from http://cdaweb.gsfc.nasa.gov/cgi-bin/eval3.cgi. This study is supported by NNFSC grants 41174145, 41231067, 41574161, and 41174144 and in part by the Specialized Research Fund for State Key Laboratories.

References

Akasofu, S.-I. (1981), Energy coupling between the solar wind and the magnetosphere, *Space Sci. Rev.*, 121–190, doi:10.1007/BF00218810.

Andrew, M. K., P. W. Daly, and E. Keppler (1981), Ion jetting at the plasma sheet boundary: Simultaneous observations of incident and reflected particle, *Geophys. Res. Lett.*, *8*, 987–990, doi:10.1029/GL008i009p00987.

Angelopoulos, V., R. C. Elphic, S. P. Gary, and C. Y. Huang (1989), Electromagnetic instabilities in the plasma sheet boundary layer, *J. Geophys. Res.*, *94*, 15,373–15,383, doi:10.1029/JA094iA11p15373.

Angelopoulos, V., W. Baumjohann, C. F. Kennel, F. V. Coroniti, M. G. Kivelson, R. Pellat, R. J. Walker, H. Lühr, and G. Paschmann (1992), Bursty bulk flows in the inner central plasma sheet, *J. Geophys. Res.*, *97*, 4027–4039, doi:10.1029/91JA02701.

Angelopoulos, V., et al. (1993), Characteristics of ion flow in the quiet state of the inner plasma sheet, *Geophys. Res. Lett.*, *20*(16), 1711–1714, doi:10.1029/93GL00847.

Angelopoulos, V., C. F. Kennel, F. V. Coroniti, R. Pellat, M. G. Kivelson, R. J. Walker, C. T. Russell, W. Baumjohann, W. C. Feldman, and J. T. Gosling (1994), Statistical characteristics of bursty bulk flow events, *J. Geophys. Res.*, *99*, 21,257–21,280, doi:10.1029/94JA01263.

Angelopoulos, V., et al. (2008), Tail reconnection triggering substorm onset, *Science*, *321*, 931, doi:10.1126/science.1160495.

Angelopoulos, V., A. Runov, X.-Z. Zhou, D. L. Turner, S. A. Kiehas, S.-S. Li, and I. Shinohara (2013), Electromagnetic energy conversion at reconnection fronts, *Science*, *341*, 1478, doi:10.1126/science.1236992.

Ashour-Abdalla, M., J. Büchner, and L. Zelenyi (1991), The quasi-adiabatic ion distribution in the central plasma sheet and its boundary layer, *J. Geophys. Res.*, *96*, 1601–1609, doi:10.1029/90JA01921.

Ashour-Abdalla, M., L. M. Zelenyi, J. M. Bosqued, and R. A. Kovrazhkin (1992), Precipitation of fast ion beams from the plasma sheet boundary layer, *Geophys. Res. Lett.*, *19*, 617–620, doi:10.1029/1992GL00048.

Baker, D. N., T. I. Pulkkinen, V. Angelopoulos, W. Baumjohann, and R. L. McPherron (1996), Neutral line model of substorms: Past results and present view, *J. Geophys. Res.*, *101*, 12,975–13,010, doi:10.1029/95JA03753.

Balogh, A., et al. (2001), The Cluster magnetic field investigation: Overview of in-flight performance and initial results, *Ann. Geophys.*, *19*, 1207–1217.

Baumjohann, W. (2002), Modes of convection in the magnetotail, *Phys. Plasmas*, *9*, 3665–3667, doi:10.1063/1.1499116.

Baumjohann, W., G. Paschmann, N. Sckopke, C. A. Cattell, and C. W. Carlson (1988), Average ion moments in the plasma sheet boundary layer, *J. Geophys. Res.*, *93*, 11,507–11,520, doi:10.1029/JA093iA10p11507.

Baumjohann, W., G. Paschmann, and C. A. Cattell (1989), Average plasma properties in the center plasma sheet, *J. Geophys. Res.*, *94*, 6597–6606, doi:10.1029/JA094iA06p06597.

Baumjohann, W., G. Paschmann, and H. Lühr (1990), Characteristics of high-speed ion flows in the plasma sheet, *J. Geophys. Res.*, *95*, 11,507–11,520, doi:10.1029/JA095iA04p03801.

Birn, J., E. Hones Jr., and K. Schindler (1986), Field-aligned plasma flow in mhd simulations of magnetotail reconnection and the formation of boundary layers, *J. Geophys. Res.*, *91*, 11,116–11,122, doi:10.1029/JA091iA10p11116.

Birn, J., J. Raeder, Y. Wang, R. Wolf, and M. Hesse (2004), On the propagation of bubbles in the geomagnetic tail, *Ann. Geophys.*, *22*, 1773–1786.

Dai, L., J. R. Wygant, C. Cattell, J. Dombeck, S. Thaller, C. Mouikis, A. Balogh, and H. Rème (2011), Cluster observations of surface waves in the ion jets from magnetotail reconnection, *J. Geophys. Res.*, *116*, A12227, doi:10.1029/2011JA017004.

Dai, L., C. Wang, V. Angelopoulos, and K.-H. Glassmeier (2015), In situ evidence of breaking the ion frozen-in condition via the non-gyrotropic pressure effect in magnetic reconnection, *Ann. Geophys.*, *33*, 1147–1153, doi:10.5194/angeo-33-1147-2015.

DeCoster, R., and L. Frank (1979), Observations pertaining to the dynamics of the plasma sheet, *J. Geophys. Res.*, *84*, 5099–5121, doi:10.1029/JA084iA09p05099.

Eastman, T. E., L. A. Frank, and C. Y. Huang (1985), The boundary layers as the primary transport regions of the Earth's magnetotail, *J. Geophys. Res.*, *90*, 9541–9560, doi:10.1029/JA090iA10p09541.
Eastman, T., L. Frank, W. Peterson, and W. Lennartsson (1984), The plasma sheet boundary layer, *J. Geophys. Res.*, *89*, 1553–1572, doi:10.1029/JA089iA03p01553.
Green, J. L., and J. L. Horwitz (1986), Destiny of earthward streaming plasma in the plasma sheet boundary layer, *Geophys. Res. Lett.*, *13*, 76–79, doi:10.1029/GL013i001p00076.
Grigorenko, E. E., J.-A. Sauvaud, and L. M. Zelenyi (2007), Spatial-temporal characteristics of ion beamlets in the plasma sheet boundary layer of magnetotail, *J. Geophys. Res.*, *112*, A05218, doi:10.1029/2006JA011986.
Grigorenko, E. E., M. Hoshino, M. Hirai, T. Mukai, and L. M. Zelenyi (2009), "Geography" of ion acceleration in the magnetotail: *X*-line versus current sheet effects, *J. Geophys. Res.*, *114*, A03203, doi:10.1029/2008JA013811.
Hones, E. W., Jr. (1973), Plasma flow in the plasma sheet and its relation to substorms, *Radio Sci.*, *8*, 979–990, doi:10.1029/RS008i011p00979.
Lennartsson, O. W., K. J. Trattner, H. L. Collin, and W. K. Peterson (2001), Polar/toroidal imaging mass-angle spectrograph survey of earthward field-aligned proton flows from the near-midnight tail, *J. Geophys. Res.*, *106*, 5859–5871, doi:10.1029/2000JA003014.
Lennartsson, O. W., L. M. Kistler, and H. Rème (2009), Cluster view of the plasma sheet boundary layer and bursty bulk flow connection, *Ann. Geophys.*, *27*, 1729–1741, doi:10.5194/angeo-27-1729-2009.
Lui, A. T. Y. (1991), A synthesis of magnetospheric substorm models, *J. Geophys. Res.*, *96*, 1849–1856, doi:10.1029/90JA02430.
Lui, A. T. Y. (1996), Current disruption in the Earth's magnetosphere: Observations and models, *J. Geophys. Res.*, *101*, 13,067–13,088, doi:10.1029/96JA00079.
Lui, A. T. Y., L. A. Frank, K. L. Ackerson, C.-I. Meng, and S.-I. Akasofu (1977a), Systematic study of plasma flow during plasma sheet thinnings, *J. Geophys. Res.*, *82*, 4815–4825.
Lui, A., E. Hones Jr., F. Yasuhara, S.-I. Akasofu, and S. Bame (1977b), Magnetotail plasma flow during plasma sheet expansions: Vela 5 and 6 and Imp 6 observations, *J. Geophys. Res.*, *82*, 1235–1244, doi:10.1029/JA082i007p01235.
Lui, A., T. Eastman, D. Williams, and L. Frank (1983), Observations of ion streaming during substorms, *J. Geophys. Res.*, *88*, 7753–7764, doi:10.1029/JA088iA10p07753.
Lyons, L. R., Y. Nishimura, X. Xing, V. Angelopoulos, S. Zou, D. Larson, J. McFadden, A. Runov, S. Mende, and K.-H. Fornacon (2010), Enhanced transport across entire length of plasma sheet boundary field lines leading to substorm onset, *J. Geophys. Res.*, *115*, A00I07, doi:10.1029/2010JA015831.
Lyons, L. R., Y. Nishimura, X. Xing, A. Runov, V. Angelopoulos, E. Donovan, and T. Kikuchi (2012), Coupling of dipolarization front flow bursts to substorm expansion phase phenomena within the magnetosphere and ionosphere, *J. Geophys. Res.*, *117*, A02212, doi:10.1029/2011JA017265.
Nakamura, M., G. Paschmann, W. Baumjohann, and N. Sckopke (1991), Ion distributions and flows near the neutral sheet, *J. Geophys. Res.*, *96*, 5631–5649, doi:10.1029/90JA02495.
Nakamura, M., W. Baumjohann, G. Paschmann, and N. Sckopke (1992), Ion distributions and flows in and near the plasma sheet boundary layer, *J. Geophys. Res.*, *97*, 1449–1460, doi:10.1029/91JA02361.
Nakamura, R., W. Baumjohann, R. Schödel, M. Brittnacher, V. A. Sergeev, M. Kubyshkina, T. Mukai, and K. Liou (2001a), Earthward flow bursts, auroral streamers, and small expansions, *J. Geophys. Res.*, *106*, 10,791–10,802, doi:10.1029/2000JA000306.
Nakamura, R., W. Baumjohann, M. Brittnacher, V. A. Sergeev, M. Kubyshkina, T. Mukai, and K. Liou (2001b), Flow bursts and auroral activations: Onset timing and foot point location, *J. Geophys. Res.*, *106*, 10,777–10,789, doi:10.1029/2000JA000249.
Nakamura, R., et al. (2002), Fast flow during current sheet thinning, *Geophys. Res. Lett.*, *29*(23), 2140, doi:10.1029/2002GL016200.
Nakamura, R., et al. (2004), Spatial scale of high-speed flows in the plasma sheet observed by Cluster, *Geophys. Res. Lett.*, *31*, L09804, doi:10.1029/2004GL019558.
Nakamura, R., W. Baumjohann, Y. Asano, A. Runov, A. Balogh, C. J. Owen, A. N. Fazakerley, M. Fujimoto, B. Klecker, and H. Rème (2006), Dynamics of thin current sheets associated with magnetotail reconnection, *J. Geophys. Res.*, *111*, A11206, doi:10.1029/2006JA011706.
Nakamura, R., et al. (2008), Cluster observations of an ion-scale current sheet in the magnetotail under the presence of a guide field, *J. Geophys. Res.*, *113*, A07S16, doi:10.1029/2007JA012760.
Nagai, T., M. Fujimoto, Y. Saito, S. Machida, T. Terasawa, R. Nakamura, T. Yamamoto, T. Mukai, A. Nishida, and S. Kokubun (1998), Structure and dynamics of magnetic reconnection for substorm onsets with Geotail observations, *J. Geophys. Res.*, *103*(A3), 4419–4440, doi:10.1029/97JA02190.
Nishimura, Y., L. R. Lyons, V. Angelopoulos, T. Kikuchi, S. Zou, and S. B. Mende (2011), Relations between multiple auroral streamers, pre-onset thin arc formation, and substorm auroral onset, *J. Geophys. Res.*, *116*, A09214, doi:10.1029/2011JA016768.
Onsager, T. G., M. F. Thomsen, R. C. Elphic, and J. T. Gosling (1991), Model of electron and ion distributions in the plasma sheet boundary layer, *J. Geophys. Res.*, *96*, 20,999–21,011, doi:10.1029/91JA01983.
Paterson, W. R., L. A. Frank, S. Kokubun, and T. Yamamoto (1998), Geotail survey of ion flow in the plasma sheet: Observations between 10 and 50 R_E, *J. Geophys. Res.*, *103*, 11,811–11,825, doi:10.1029/97JA02881.
Petrukovich, A. A., W. Baumjohann, R. Nakamura, R. Schödel, and T. Mukai (2001), Are earthward bursty bulk flows convective or field-aligned?, *J. Geophys. Res.*, *106*, 21,211–21,215, doi:10.1029/2001JA900019.
Petrukovich, A. A., W. Baumjohann, R. Nakamura, A. Runov, A. Balogh, and H. Re'me (2007), Thinning and stretching of the plasma sheet, *J. Geophys. Res.*, *112*, A10213, doi:10.1029/2007JA012349.
Raj, A., T. Phan, R. P. Lin, and V. Angelopoulos (2002), Wind survey of high-speed bulk flows and field-aligned beams in the near-Earth plasma sheet, *J. Geophys. Res.*, *107*(A12), 1419, doi:10.1029/2001JA007547.
Rème, H., et al. (2001), First multispacecraft ion measurements in and near the Earth 's magnetosphere with the identical CLUSTER Ion Spectrometry (CIS) Experiment, *Ann. Geophys.*, *19*(10–12), 1303–1354.
Runov, A., et al. (2003), Current sheet structure near magnetic X-line observed by Cluster, *Geophys. Res. Lett.*, *30*(11), 1579, doi:10.1029/2002GL016730.
Sarris, E., D. Williams, and S. Krimigis (1978), Observations of Counterstreaming between Plasma and Energetic Particles in the Magnetotail, *J. Geophys. Res.*, *83*, 5655–5662, doi:10.1029/JA083iA12p05655.
Schindler, K., and J. Birn (1987), On the generation of field-aligned plasma flow at the boundary of the plasma sheet, *J. Geophys. Res.*, *92*, 95–107, doi:10.1029/JA092iA01p00095.
Schödel, R., W. Baumjohann, R. Nakamura, V. A. Sergeev, and T. Mukai (2001), Rapid flux transport in the central plasma sheet, *J. Geophys. Res.*, *106*, 301–314, doi:10.1029/2000JA900139.
Shiokawa, K., W. Baumjohanna, and G. Haerendel (1997), Braking of high-speed flows in the near-Earth tail, *Geophys. Res. Lett.*, *24*, 1179–1182, doi:10.1029/97GL01062.
Shiokawa, K., et al. (1998), High-speed ion flow, substorm current wedge, and multiple Pi2 pulsations, *J. Geophys. Res.*, *103*, 4491–4507, doi:10.1029/1997JA01680.
Takahashi, K., and E. Hones Jr. (1988), ISEE 1 and 2 observations of ion distributions at the plasma sheet-tail lobe boundary, *J. Geophys. Res.*, *93*, 8558–8582, doi:10.1029/JA093iA08p08558.

Williams, D. J. (1981), Energetic ion beams at the edge of the plasma sheet: ISSE 1 observations plus a simple explanatory model, *J. Geophys. Res.*, *86*, 5507–5518, doi:10.1029/JA086iA07p05507.

Zhang, L. Q., et al. (2009), Convective bursty flows in the near-Earth magnetotail inside 13 R_E, *J. Geophys. Res.*, *114*, A02202, doi:10.1029/2008JA013125.

Zhang, L. Q., Z. X. Liu, Z. W. Ma, W. Baumjohann, Z. Y. Pu, M. W. Dunlop, H. Reme, and J. Y. Wang (2010), X line distribution determined from earthward and tailward convective bursty flows in the central plasma sheet, *J. Geophys. Res.*, *115*, A06218, doi:10.1029/2009JA014429.

Zhang, L. Q., A. T. Y. Lui, W. Baumjohann, and J. Y. Wang (2015a), Probabilities of magnetic reconnection encounter at different activity levels in the Earth's magnetotail, *Adv. Space Res.*, *56*, 736–741, doi:10.1016/ja.asr.2015,05.001.

Zhang, L. Q., W. Baumjohann, J. Y. Wang, H. Rème, M. W. Dunlop, and T. Chen (2015b), Statistical characteristics of slow earthward and tailward flows in the plasma sheet, *J. Geophys. Res. Space Physics*, *120*, 6199–6206, doi:10.1002/2015JA021354.

Zhou, X.-Z., V. Angelopoulos, A. Runov, J. Liu, and Y. S. Ge (2012), Emergence of the active magnetotail plasma sheet boundary from transient, localized ion acceleration, *J. Geophys. Res.*, *117*, A10216, doi:10.1029/2012JA018171.